J Mol Model (2013) 19:1515–1525
DOI 10.1007/s00894-012-1704-9

ORIGINAL PAPER

Theoretical study and rate constant calculations for the reactions of $SiHX_3$ with CF_3 and CH_3 radicals (X = F, Cl)

Hui Zhang · Ping Liu · Jing-Yao Liu · Ze-Sheng Li

Received: 16 June 2012 / Accepted: 19 November 2012 / Published online: 21 December 2012

Abstract Theoretical investigations were carried out on the multi-channel reactions CF_3 + $SiHF_3$, CF_3 + $SiHCl_3$, CH_3 + $SiHF_3$, and CH_3 + $SiHCl_3$. Electronic structures were calculated at the MP2/6-311+G(d,p) level, and energetic information further refined by the MC-QCISD (single-point) method. The rate constants for major reaction channels were calculated by the canonical variational transition state theory with small-curvature tunneling correction over the temperature range of 200–1,500 K. The theoretical rate constants were in good agreement with the available experimental data and were fitted to the three parameter expression: $k_{1a}(T) = 2.93 \times 10^{-26}\ T^{4.25}$ exp $(-318.68/T)$, and $k_{2a}(T) = 3.67 \times 10^{-22}\ T^{2.72}$ exp $(-1{,}414.22/T)$, $k_{3a}(T) = 7.00 \times 10^{-24}\ T^{3.27}$ exp $(-384.04/T)$, $k_{4a}(T) = 6.35 \times 10^{-22}\ T^{2.59}$ exp $(-603.18/T)$ (in unit of $cm^3molecule^{-1}s^{-1}$) are given. Our calculations indicate that hydrogen abstraction channel is the major channel due to the smaller barrier height among four channels considered.

H. Zhang (✉) · P. Liu
College of Chemical and Environmental Engineering, Harbin University of Science and Technology, Harbin 150080, People's Republic of China
e-mail: hust_zhanghui11@hotmail.com

J.-Y. Liu
Institute of Theoretical Chemistry, Jilin University, Changchun 130023, People's Republic of China

Z.-S. Li (✉)
Academy of Fundamental and Interdisciplinary Sciences, Department of Chemistry, Harbin Institute of Technology, Harbin 150080, People's Republic of China
e-mail: zeshengli@bit.edu.cn

Z.-S. Li
Key Laboratory of Cluster Science of Ministry of Education and School of Chemistry, Beijing Institute of Technology, Beijing 100081, People's Republic of China

Keywords Gas-phase reaction · Transition state · Rate constant

Introduction

Silicon is in the same family of elements as carbon in the periodic table, but is metallic in character and more electropositive than carbon (2.55) and hydrogen (2.20). Therefore, silicon-based chemicals exhibit significant physical and chemical differences compared to analogous carbon-based chemicals, which makes it interesting to study the kinetics and mechanisms of small silicon-containing molecules [1–7]. Silane and its halogen-substituted homolog are considered as important reagents in a wide variety of materials synthesis processes. For example, these compounds are used to deposit silicon carbide (SiC) by chemical vapor deposition (CVD), in glow discharge deposition of amorphous silicon films, and in semiconductor manufacturing processes [8–13]. However, the use of volatile silicon compounds may lead to their emission into the atmosphere, where they can be removed by reactions with a variety of reactive species. Thus, the kinetics and mechanisms of small silicon-containing molecules attract considerable interest [7]. The use of volatile silicon compounds may lead to their emission into the atmosphere, where they can be removed by reaction with a variety of reactive species.

Two classes of reaction channels will happen when $SiHF_3$ and $SiHCl_3$ react with CF_3 and CH_3 radicals: one is that the hydrogen and halogen atoms in $SiHF_3$ and $SiHCl_3$ are abstracted; the other is that the hydrogen atom and the halogen atom are substituted by CF_3 and CH_3 radicals. As a result, four reaction channels are feasible, denoted as R1a (R2a, R3a, R4a), R1b (R2b, R3b, R4b), R1c (R2c, R3c, R4c), and R1d (R2d, R3d, R4d), respectively, as follows:

$$CF_3 + SiHF_3 \rightarrow SiF_3 + CHF_3\,(R1a)$$
$$\rightarrow SiF_3CF_3 + H\,(R1a)$$
$$\rightarrow SiHF_2 + CF_4(R1c)$$
$$\rightarrow SiHF_2CF_3 + F(R1d)$$

$$CH_3 + SiHF_3 \rightarrow SiF_3 + CH_4(R2a)$$
$$\rightarrow SiF_3CH_3 + H(R2b)$$
$$\rightarrow SiHF_2 + CH_3F(R2c)$$
$$\rightarrow SiHF_2CH_3 + F(R2d)$$

$$CF_3 + SiHCl_3 \rightarrow SiCl_3 + CHF_3(R3a)$$
$$\rightarrow SiCl_3CF_3 + H\,(R3b)$$
$$\rightarrow SiHCl_2 + CF_3Cl(R3c)$$
$$\rightarrow SiHCl_2CF_3 + Cl(R3d)$$

$$CH_3 + SiHCl_3 \rightarrow SiCl_3 + CH_4(R4a)$$
$$\rightarrow SiCl_3CH_3 + H(R4b)$$
$$\rightarrow SiHCl_2 + CH_3Cl(R4c)$$
$$\rightarrow SiHCl_2CH_3 + Cl(R4d)$$

Limited kinetic works have focused on those reactions despite their practical and theoretical importance. Six papers have reported experimental kinetic data on the title reactions. Arrhenius parameters have been obtained for the reaction CH_3 + $SiHF_3$ → SiF_3 + CH_4 (R2a) over a temperature range of 343—470 K by Kerr and co-workers [14]: Arrhenius expression of 3.72×10^{-12} exp[–36417(±728 J/mole)/RT] $cm^3molecule^{-1}s^{-1}$ is given with the value of 3.34×10^{-16} cm^3 $molecule^{-1}s^{-1}$ at 470 K. As for the reaction CF_3 + $SiHCl_3$ → $SiCl_3$ + CHF_3 (R3a), rate constants have been reported [15–18] over a temperature range of 323—567 K. For the reaction CH_3 + $SiHCl_3$ → $SiCl_3$ + CH_4 (R4a), rate constants have been determined [16, 19] over a temperature range of 303—443 K. No experimental information is available on the higher temperature of the title reactions; theoretical investigation is desirable to provide further understanding of the mechanism of these multi-channel reactions and to evaluate the rate constant at higher temperatures. To the best of our knowledge, no theoretical work has been performed on the kinetics of the title reactions.

In this paper, a dual-level (X//Y) direct dynamics method [20–24] was employed to study the kinetics of the reactions of $SiHF_3$ and $SiHCl_3$ with CF_3 and CH_3 radicals. The potential energy surface information, including geometries, energies, gradients, force constants of all the stationary points (reactants, products, and transition states) and plus selected 16 points (8 points on each side of saddle point) along the minimum energy path (MEP), was obtained directly from ab initio calculations. Single-point energies are calculated by the MC-QCISD method [25]. Subsequently, by means of the POLYRATE 9.7 program, [26] the rate constants of the four reaction channels were calculated by the variational transition state theory (VTST) [27, 28] proposed by Truhlar and coworkers. The comparison between the theoretical and experimental results is discussed. Our results may be helpful for further experimental investigations.

Computational methods

In the present work, the equilibrium geometries and frequencies of all the stationary points (reactants, products, and transition states) were optimized at the restricted or unrestricted second-order Møller-Plesset perturbation (MP2) [29–31] level with the 6-311+G(d,p) basis set. Molecular electrostatic potentials [32] of reactants $SiHF_3$, $SiHCl_3$, CF_3 and CH_3 are calculated at the same level, and plotted using gOpenMol 2.32 [33]. The MEP is obtained by intrinsic reaction coordinate (IRC) theory with a gradient step-size of 0.05 $(amu)^{1/2}$ bohr. Then, the first and second energy derivatives are obtained to calculate the curvature of the reaction path and the generalized vibrational frequencies along the reaction path. In order to obtain more accurate energies and barrier heights, the energies are refined by the MC-QCISD method (multi-coefficient correlation method based on quadratic configuration interaction with single and double excitations proposed by Fast and Truhlar) [25] based on the MP2/6-311+G(d,p) geometries. All the electronic structure calculations are performed by the GAUSSIAN09 program package [34].

Based on the above information, the rate constants were evaluated by the VTST [27, 28] theory over a temperature range of 200–1,500 K. The dynamics calculation are performed by the POLYRATE 9.7 program [26]. The specific level used in this work is the canonical variational transition state theory (CVT) [35–37] incorporating small-curvature tunneling (SCT) [38, 39] contributions proposed by Truhlar and coworkers [35]. For the four reaction channel transitional state modes, the four lowest frequencies are treated as a hindered internal rotation using the hindered-rotor approximation developed by Truhlar and Chuang [40, 41], other vibrational modes are treated as quantum-mechanical separable harmonic oscillators. The curvature components are calculated by using a quadratic fit to obtain the derivative of the gradient with respect to the reaction coordinate.

Results and discussion

Stationary points

The optimized geometries of the reactants (CF_3, CH_3, $SiHF_3$, and $SiHCl_3$), products (SiF_3, CHF_3, SiF_3CF_3, $SiHF_2$,

CF_4, $SiHF_2CF_3$, CH_4, SiF_3CH_3, CH_3F, $SiHF_2CH_3$, $SiCl_3$, $SiCl_3CF_3$, $SiHCl_2$, CF_3Cl, $SiHCl_2CF_3$, $SiCl_3CH_3$, CH_3Cl, and $SiHCl_2CH_3$), and transition states (TS1a–d, TS2a–d, TS3a–d, and TS4a–d) calculated at the MP2/6-311+G(d,p) level are presented in Fig. 1, along with the available experimental values. [42] The theoretical geometric parameters of CF_3, CH_3, CH_4, CH_3F, CHF_3, CH_3Cl, and CF_4 are in good agreement with the corresponding experimental values [42]. Figure 1 shows that the transition states TS1a, TS2a, TS3a, and TS4a have the same symmetry, C_S. In

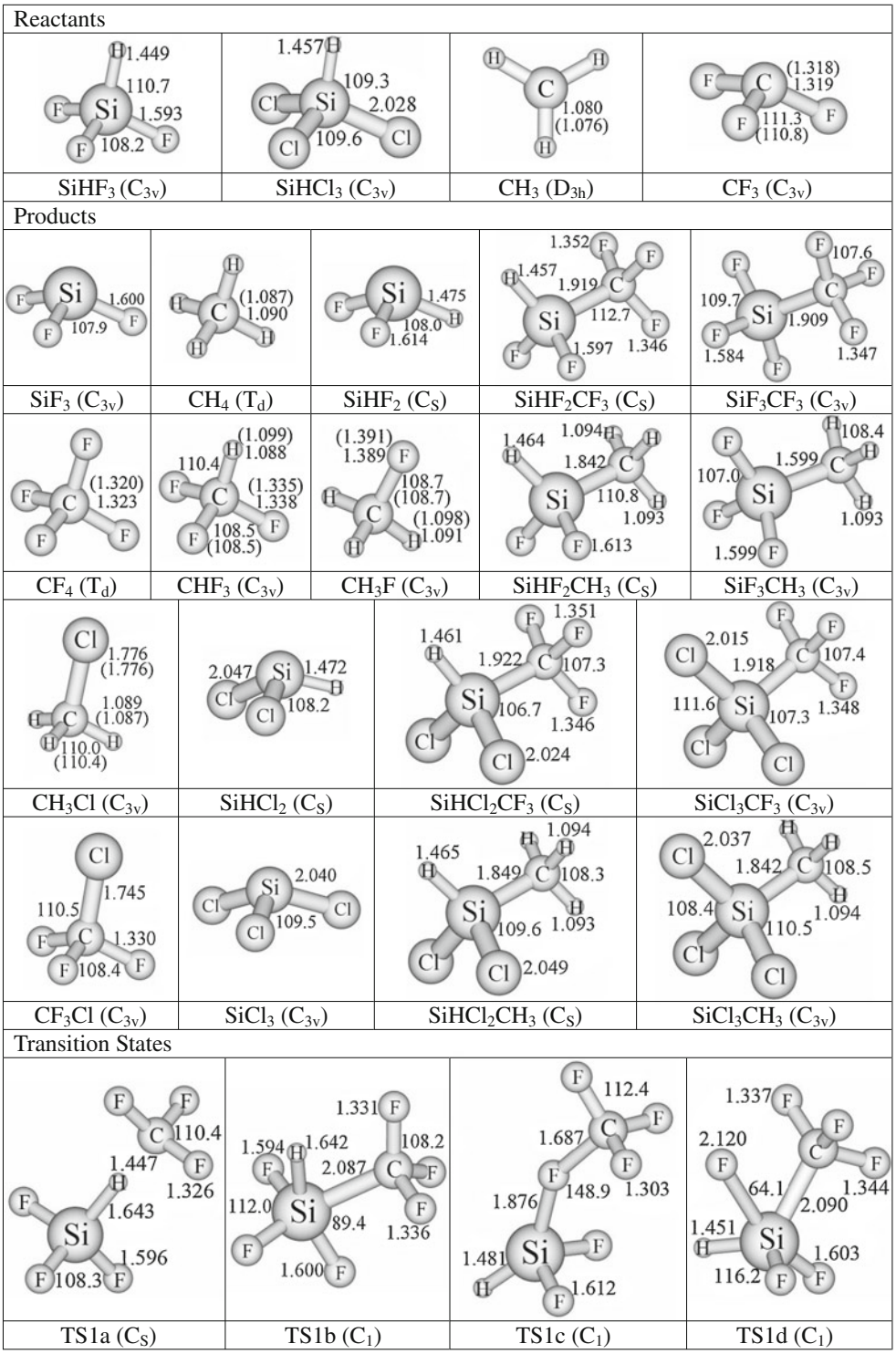

Fig. 1 Optimized geometries of the reactants, products, and transition states at the MP2/6-311+G(d,p) level. The values in parentheses are the experimental values (ref. [42] for CF_3, CH_3, CH_4, CH_3F, CHF_3, and CF_4). Bond lengths are in Ångstroms and angles are in degrees

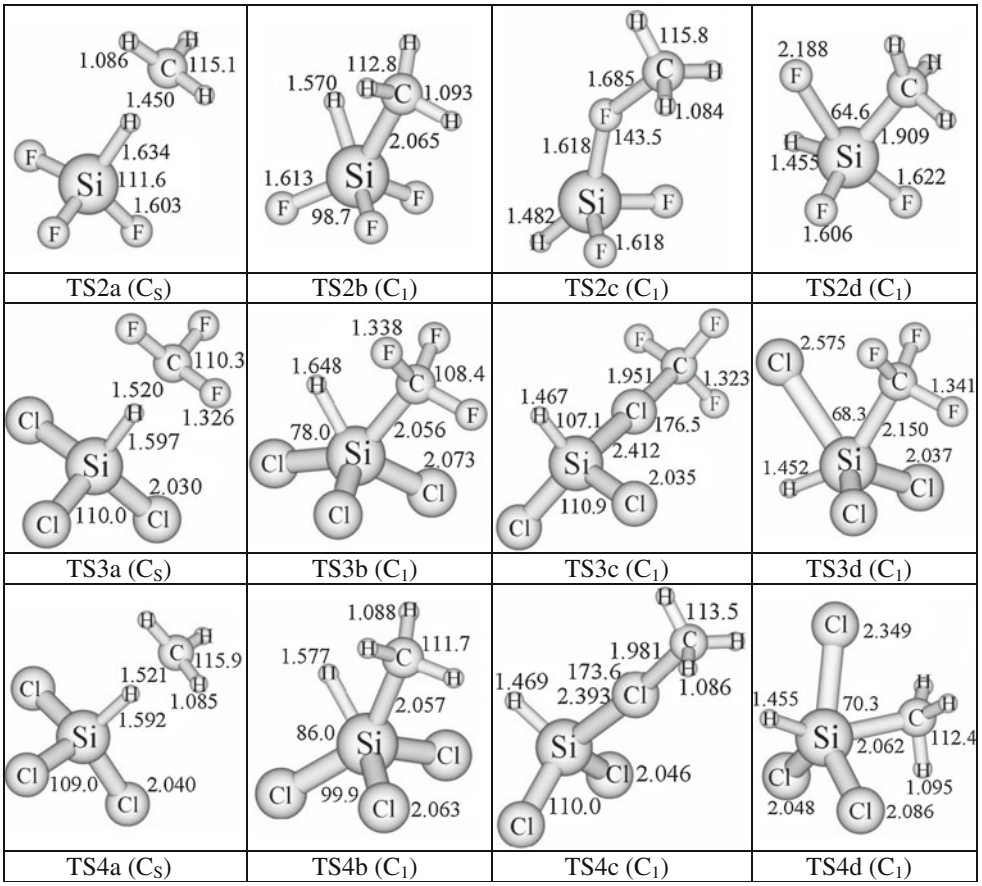

Fig. 1 continued.

TS1a, TS2a, TS2b, TS3a, TS4a, and TS4b structures, the breaking bonds Si—H are increased by 13 %, 8 %, 9 %, 10 %, 9 %, and 8 % compared to the equilibrium bond length in $SiHF_3$ and $SiHCl_3$; the forming bonds C—H and C—Si are stretched by 33 %, 29 %, 30 %, 40 %, 40 %, and 12 % over the equilibrium bond lengths in isolated CHF_3, CH_4, SiF_3CH_3, and $SiCl_3CH_3$, respectively. The elongation of the breaking bond is smaller than that of the forming bond, indicating that the above-mentioned reaction channels are all reactant-like, i.e., the three reaction channels will proceed via "early" transition states. According to Hammond's postulate [43] they will be exothermic reactions.

Table 1 lists the harmonic vibrational frequencies of the reactants, products, and transition states calculated at the MP2/6-311+G(d,p) level as well as the available experimental values [44, 45]. For the species CF_3, CH_3, $SiHF_3$, SiF_3, CH_4, CH_3F, CH_3Cl, CHF_3, CF_3Cl, and CF_4, the calculated frequencies are in agreement with the experimental values with the largest deviation within 6 %. The 16 transition states are all confirmed by normal-mode analysis to have one and only one imaginary frequency, which corresponds to the stretching modes of coupling between breaking and forming bonds.

Energetics

The reaction enthalpies $\left(\Delta H^0_{298}\right)$ and potential barrier heights (ΔE^{TS}) with zero-point energy (ZPE) corrections for all reaction channels calculated at the MC-QCISD//MP2/6-311+G(d,p) level are listed in Table 2. The theoretical values at 298 K of ΔH^0_{298} for reactions R1a-4a and R1a-4c are in good agreement with the corresponding experimental values, which are derived from the standard heats of formation (CF_3, −112.32 kcal mol^{-1} [46]; $SiHF_3$, −286.85±0.48 kcal mol^{-1} [7]; SiF_3, −238.85 ±1.19 kcal mol^{-1} [7]; CHF_3, −166.49 kcal mol^{-1} [46]; $SiHF_2$, −139.96±1.43 kcal mol^{-1} [7]; CF_4, −222.40 kcal mol^{-1} [47]; CH_3, 34.80 kcal mol^{-1} [46]; CH_4, −17.88 kcal mol^{-1} [47]; CH_3F, −55.96 kcal mol^{-1} [46]; $SiHCl_3$, −115.12 kcal mol^{-1} [7]; $SiHCl_2$, −33.40±1.40 kcal mol^{-1} [48]; $SiCl_3$, −75.5 kcal mol^{-1} [48]; CH_3Cl, −19.56±0.36 kcal mol^{-1} [49]; CF_3Cl, −69.58 ±7.17 kcal mol^{-1} [47]), which indicates the values calculated at the MC-QCISD//MP2/6-311+G(d,p) level may be reliable. Thus, we use MC-QCISD//MP2/6-311+G(d,p) method to calculate the potential energy barriers as well as the energies along the MEP in the following studies. From Table 2, it is also shown that the R1a, R2a, R2b, R3a, R4a, and R4b reaction channels are all exothermic reactions, consistent with Hammond's postulate [43].

Table 1 Calculated and experimental frequencies (in cm^{-1}) for the reactants, products, and transition states for the title reaction at the MP2/6-311+G(d,p) level

Species	MP2/6-311+G(d,p)	Experimental
CH_3	3362, 3362, 3169, 1446, 1446, 459	[a]3171, 3004, 1403
CF_3	1272, 1272, 1106, 711, 516, 516	[a]1260, 1089, 703, 512
$SiHF_3$	2454, 981, 981, 858, 858, 839, 415, 302, 302	[b]2316, 998, 858, 844, 425, 306
$SiHCl_3$	2407, 843, 843, 618, 618, 508, 264, 186, 186	[b]2261, 811, 600, 499, 254, 176
SiF_3	946, 946, 821, 403, 290, 290	[a]954, 832, 406, 290
$SiCl_3$	604, 604, 490, 255, 177, 177	[a]582, 470
CH_4	3211, 3211, 3211, 3074, 1575, 1575, 1363, 1363, 1363	[b]3019, 2917, 1534
$SiHF_2$	2288, 917, 846, 791, 783, 308	
$SiHCl_2$	2311, 795, 697, 592, 530, 190	
CH_3F	3197, 3197, 3093, 1522, 1522, 1517, 1217, 1217, 1076	[b]3006, 2930, 1467, 1464, 1182, 1049
SiF_3CH_3	3191, 3191, 3092, 1470, 1470, 1336, 969, 969, 902, 809, 809, 699, 380, 323, 323, 216, 216, 140	
$SiHF_2CH_3$	3182, 3179, 3083, 2375, 1469, 1466, 1328, 958, 949, 864, 855, 792, 762, 686, 339, 280, 223, 139	
$SiHCl_2CF_3$	2394, 1251, 1143, 1131, 831, 802, 742, 636, 562, 529, 528, 425, 286, 268, 182, 128, 100, 42	
CHF_3	3221, 1424, 1424, 1176, 1176, 1151, 704, 513, 513	[b]3036, 1372, 1152, 1117, 700, 507
CF_4	1288, 1288, 1288, 912, 634, 634, 634, 441, 441	[b]1281, 909, 632, 435
CF_3Cl	1221, 1221, 1132, 795, 567, 567, 493, 360, 360	[b]1212, 1105, 781, 563, 476, 350
CH_3Cl	3220, 3220, 3113, 1494, 1494, 1443, 1067, 1067, 786	[b]3039, 2937, 1452, 1355, 1017, 732
SiF_3CF_3	1274, 1147, 1147, 1002, 1002, 855, 740, 533, 533, 489, 352, 352, 260, 253, 253, 126, 126, 35	
$SiCl_3CF_3$	1247, 1143, 1143, 753, 658, 658, 550, 529, 529, 375, 285, 285, 181, 181, 179, 99, 99, 43	
$SiCl_3CH_3$	3181, 3181, 3080, 1455, 1455, 1328, 833, 833, 783, 598, 598, 462, 240, 221, 221, 189, 160, 160	
$SiHF_2CF_3$	2418, 1271, 1143, 1128, 972, 886, 839, 829, 740, 537, 528, 445, 363, 289, 253, 156, 122, 39	
$SiHCl_2CH_3$	3181, 3174, 3078, 2364, 1459, 1458, 1326, 922, 889, 780, 777, 698, 583, 513, 250, 187, 186, 175	
TS1a	1285, 1285, 1176, 1176, 1115, 959, 959, 826, 733, 516, 516, 431, 300, 300, 196, 141, 141, 49, 49, 16, 1855*i*	
TS1b	1353, 1213, 1191, 1050, 979, 925, 838, 774, 643, 555, 535, 505, 434, 351, 297, 236, 217, 200, 51, 37, 595*i*	
TS1c	2230, 1348, 1348, 1027, 920, 834, 777, 752, 734, 550, 546, 416, 385, 360, 296, 193, 191, 63, 59, 9, 1235*i*	
TS1d	2437, 1201, 1138, 1035, 959, 927, 863, 768, 726, 546, 525, 420, 351, 289, 277, 260, 246, 226, 78, 48, 660*i*	
TS2a	3282, 3282, 3117, 1455, 1455, 1172, 1172, 1146, 938, 938, 826, 499, 499, 484, 320, 294, 293, 61, 61, 14, 1687*i*	
TS2b	3263, 3231, 3088, 1640, 1472, 1424, 1132, 1007, 950, 888, 840, 816, 710, 627, 431, 373, 323, 259, 162, 78, 388*i*	
TS2c	3313, 3308, 3143, 2314, 1474, 1472, 1226, 899, 897, 881, 859, 822, 801, 410, 322, 296, 251, 84, 72, 51, 1368*i*	
TS2d	3197, 3174, 3062, 2415, 1463, 1417, 1240, 969, 930, 857, 828, 746, 703, 630, 365, 332, 311, 226, 161, 119, 495*i*	
TS3a	1253, 1253, 1119, 1108, 1108, 754, 621, 621, 515, 515, 511, 318, 187, 187, 160, 117, 117, 34, 34, 12, 1506*i*	
TS3b	1225, 1182, 1173, 983, 777, 639, 619, 546, 534, 524, 422, 379, 305, 281, 214, 203, 164, 144, 75, 56, 495*i*	
TS3c	2343, 1248, 1247, 1029, 809, 722, 699, 609, 541, 540, 533, 302, 295, 243, 204, 126, 125, 41, 29, 4, 564*i*	
TS3d	2423, 1241, 1238, 1038, 862, 854, 728, 623, 564, 553, 491, 392, 285, 282, 216, 204, 164, 149, 85, 48, 423*i*	
TS4a	3293, 3293, 3124, 1450, 1450, 1127, 1097, 1097, 611, 611, 583, 477, 477, 401, 223, 180, 180, 49, 49, 42, 1346*i*	

Table 1 (continued)

Species	MP2/6-311+G(d,p)	Experimental
TS4b	3242, 3212, 3075, 1551, 1461, 1421, 1166, 962, 858, 786, 612, 521, 487, 462, 328, 259, 241, 190, 179, 95, 356*i*	
TS4c	3276, 3276, 3125, 2330, 1464, 1463, 1237, 863, 855, 808, 719, 593, 527, 335, 214, 154, 148, 48, 23, 16, 586*i*	
TS4d	3274, 3220, 3076, 2395, 1465, 1393, 1218, 1005, 864, 831, 769, 575, 494, 431, 335, 293, 281, 192, 162, 43, 267*i*	

[a] Ref. [44]

[b] Ref. [45]

Table 3 lists the calculated bond dissociation energies D^o_{298} of the Si—H, Si—F and Si—Cl bonds in $SiHF_3$, $SiHCl_3$, and related compounds, along with several experimental data [50–54]. The D^o_{298} (Si—H) values of $SiHF_3$, SiH_4, and $SiHCl_3$ obtained at the MC-QCISD//MP2/6-311+G(d,p) level show good consistency with the previous literature results, 99.84 [50], 88.85 [50], and 91.30±1.20 kcal mol^{-1} [52], respectively. At the same level, the D^o_{298} (Si—F) values in SiH_3F and SiF_4 compare quite well with the corresponding experimental results, 150.22 [51] and 169.82 kcal mol^{-1} [50], respectively. Similarly, the D^o_{298}(Si—Cl) values in $SiCl_4$ and SiH_3Cl, also agree well with the corresponding experimental results, 111.30 ±1.00 [53] and 109.50±1.70 kcal mol^{-1} [54], respectively. No comparison between theory and experiment can be made due to the lack of the experimental D^o_{298} (Si—H) value in SiH_3F, SiH_3Cl, D^o_{298} (Si—F) value in $SiHF_3$, and D^o_{298} (Si—Cl) value in $SiHCl_3$. The good agreement between the theoretical and experimental D^o_{298} (Si—H), D^o_{298} (Si—F), and D^o_{298} (Si—Cl) implies that the MC-QCISD//MP2/6-311+G(d,p) level is a reliable method to compute the bond dissociation energies and our calculated D^o_{298} (Si—H) value in SiH_3F, D^o_{298} (Si—F) value in $SiHF_3$, and D^o_{298} (Si—Cl) value in $SiHCl_3$ may be expected to provide reliable reference information for future laboratory investigations. The dissociation energy of the Si—H bonds are 67.49 and 21.35 kcal mol^{-1} smaller than that of the Si—F and Si—Cl bonds in $SiHF_3$ and $SiHCl_3$, respectively, indicating that the H-abstraction channel will be more favorable than the F-abstraction and Cl-abstraction channels.

The schematic potential energy diagrams of $SiHF_3$ and $SiHCl_3$ with CF_3 and CH_3 reactions with ZPE corrections obtained at the MC-QCISD//MP2/6-311+G(d,p) level are plotted in Figs. 2, 3, 4 and 5, respectively. Note that the energy of reactant is set to be zero as a reference. The values in parentheses are calculated at the MP2/6-311+G(d,p) level including the ZPE corrections. The potential barrier height of reaction channel R1a (10.67 kcal mol^{-1}) and is much lower than those of R1b (27.44 kcal mol^{-1}), R1c (71.39 kcal mol^{-1}), and R1d (83.80 kcal mol^{-1}) at the MC-QCISD//MP2/6-311 +G(d,p) level. At the same time, reaction R1a is more exothermic than those of reactions R1b, R1c, and R1d by about 15.46, 43.36, and 84.43 kcal mol^{-1}, respectively. Compared with the reaction channels R1b and R1c, the reaction channel R1a is most exothermic and has the lowest barrier height. As a result, the reaction channel R1a is favorable both thermodynamically and kinetically. The channel R1a will dominate the reaction $CF_3 + SiHF_3$, and the contribution coming from other paths can be negligible. Similar behavior can be found for other three reactions, i.e., $SiHF_3$ with CH_3 radical, $SiHCl_3$ with CF_3 radical, $SiHCl_3$ with CH_3 radical, which indicates that the reaction channels R2b, R2c, R2d, R3b, R3c, R3d, R4b, R4c, and R2d can also be negligible. So only the rate constants for the H-abstraction channels R1a, R2a, R3a, and R4a are performed in the following section.

Table 2 The reaction enthalpies at 298 K $\left(\Delta H^0_{298}\right)$, barrier heights TSs ($\Delta E^{TS}$) (kcal mol^{-1}) with zero-point energy (ZPE) correction for the reactions $SiHF_3$ with CF_3 and CH_3 radicals at the MC-QCISD//MP2/6-311+G(d,p) level together with the experimental values

		MC-QCISD//MP2	Experimental[a]
ΔH^0_{298}	$CF_3 + SiHF_3 \rightarrow SiF_3 + CHF_3$ (R1a)	–7.50	–6.17±1.43
	$CF_3 + SiHF_3 \rightarrow SiF_3CF_3 + H$ (R1b)	7.96	
	$CF_3 + SiHF_3 \rightarrow SiHF_2 + CF_4$ (R1c)	35.86	36.81±5.21
	$CF_3 + SiHF_3 \rightarrow SiHF_2CF_3 + F$ (R1d)	76.93	
	$CH_3 + SiHF_3 \rightarrow SiF_3 + CH_4$ (R2a)	–4.83	–4.68±1.43
	$CH_3 + SiHF_3 \rightarrow SiF_3CH_3 + H$ (R2b)	–3.00	
	$CH_3 + SiHF_3 \rightarrow SiHF_2 + CH_3F$ (R2c)	54.81	56.13±1.91
	$CH_3 + SiHF_3 \rightarrow SiHF_2CH_3 + F$ (R2d)	68.85	
	$CF_3 + SiHCl_3 \rightarrow SiCl_3 + CHF_3$ (R3a)	–14.94	–14.55
	$CF_3 + SiHCl_3 \rightarrow SiCl_3CF_3 + H$ (R3b)	4.65	
	$CF_3 + SiHCl_3 \rightarrow SiHCl_2 + CF_3Cl$ (R3c)	25.39	24.46±8.57
	$CF_3 + SiHCl_3 \rightarrow SiHCl_2CF_3 + Cl$ (R3d)	25.83	
	$CH_3 + SiHCl_3 \rightarrow SiCl_3 + CH_4$ (R4a)	–12.27	–13.06
	$CH_3 + SiHCl_3 \rightarrow SiCl_3CH_3 + H$ (R4b)	–3.17	
	$CH_3 + SiHCl_3 \rightarrow SiHCl_2 + CH_3Cl$ (R4c)	29.14	27.36±1.76
	$CH_3 + SiHCl_3 \rightarrow SiHCl_2CH_3 + Cl$ (R4d)	19.21	
ΔE^{TS}+ZPE	$CF_3 + SiHF_3 \rightarrow SiF_3 + CHF_3$ (R1a)	10.67	
	$CF_3 + SiHF_3 \rightarrow SiF_3CF_3 + H$ (R1b)	27.44	
	$CF_3 + SiHF_3 \rightarrow SiHF_2 + CF_4$ (R1c)	71.39	
	$CF_3 + SiHF_3 \rightarrow SiHF_2CF_3 + F$ (R1d)	83.80	
	$CH_3 + SiHF_3 \rightarrow SiF_3 + CH_4$ (R2a)	12.69	
	$CH_3 + SiHF_3 \rightarrow SiF_3CH_3 + H$ (R2b)	22.11	
	$CH_3 + SiHF_3 \rightarrow SiHF_2 + CH_3F$ (R2c)	76.47	
	$CH_3 + SiHF_3 \rightarrow SiHF_2CH_3 + F$ (R2d)	71.88	
	$CF_3 + SiHCl_3 \rightarrow SiCl_3 + CHF_3$ (R3a)	5.42	
	$CF_3 + SiHCl_3 \rightarrow SiCl_3CF_3 + H$ (R3b)	23.15	
	$CF_3 + SiHCl_3 \rightarrow SiHCl_2 + CF_3Cl$ (R3c)	30.91	
	$CF_3 + SiHCl_3 \rightarrow SiHCl_2CF_3 + Cl$ (R3d)	44.61	
	$CH_3 + SiHCl_3 \rightarrow SiCl_3 + CH_4$ (R4a)	7.65	
	$CH_3 + SiHCl_3 \rightarrow SiCl_3CH_3 + H$ (R4b)	20.89	
	$CH_3 + SiHCl_3 \rightarrow SiHCl_2 + CH_3Cl$ (R4c)	34.52	
	$CH_3 + SiHCl_3 \rightarrow SiHCl_2CH_3 + Cl$ (R4d)	33.40	

[a]Experimental value derived from the standard heats of formation (in kcal mol^{-1}): CF_3 −112.32 [46]; $SiHF_3$ −286.85 ±0.48 [7]; SiF_3 −238.85±1.19 [7]; CHF_3 −166.49; [46]; $SiHF_2$ −139.96±1.43 [7]; CF_4 −222.40 [47]; CH_3 34.80 [46]; CH_4 −17.88 [47]; CH_3F −55.96 [46]; $SiHCl_3$ −115.12 [7]; $SiHCl_2$ −33.40±1.40 [48]; $SiCl_3$ −75.5 [48]; CH_3Cl −19.56±0.36; [49] CF_3Cl −69.58±7.17 [47]

Rate constants

Dual-level dynamics calculations [20–24] for R1a-4a reaction channels were carried out at the MC-QCISD//MP2/6-311+G(d,p) level. The rate constants of the four channels, k_{1a}, k_{2a}, k_{3a}, and k_{4a}, were evaluated by the conventional transition state theory (TST), the canonical variational transition state theory (CVT), and the CVT with the small-

Table 3 Calculated and experimental bond dissociation energies (kcal mol^{-1}) in $SiHF_3$ and $SiHCl_3$ at 298 K at MC-QCISD//MP2/6-311+G(d,p) level and related compounds

	$SiHF_3$	SiH_3F	SiH_4	SiF_4	$SiHCl_3$	$SiCl_4$	SiH_3Cl
D^o_{298} (Si—H)	98.50	92.13	89.79		91.05		90.11
Exptl.	99.84 [50]		88.85 [50]		91.30±1.20 [52]		
D^o_{298} (Si—F)	165.99	151.57		167.07			
Experimental		150.22 [51]		169.82 [50]			
D^o_{298} (Si—Cl)					112.40	111.90	108.85
Experimental						111.30±1.00 [53]	109.50±1.70 [54]

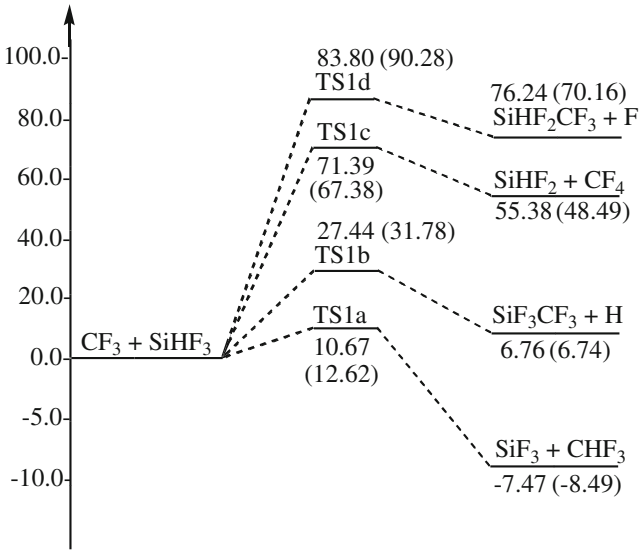

Fig. 2 Schematic potential energy surface for the reaction CF_3 + $SiHF_3$. Relative energies are calculated at the MC-QCISD//MP2/6-311+G(d,p) + ZPE level (in kcal mol^{-1}). Values in parentheses are calculated at the MP2/6-311+G(d,p) + ZPE level

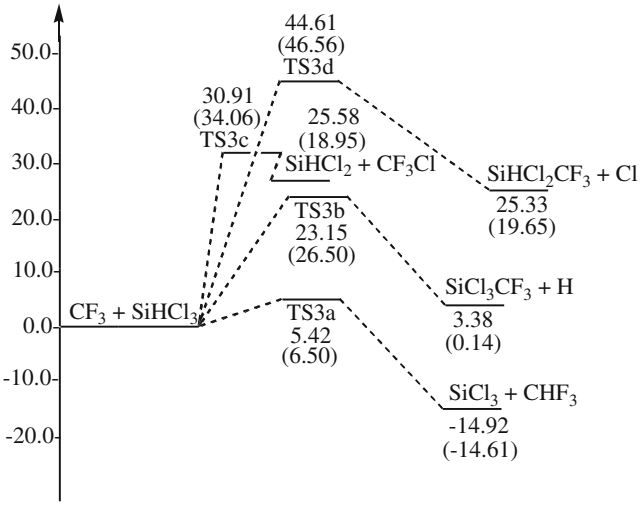

Fig. 4 Schematic potential energy surface for the reaction CF_3 + $SiHCl_3$. Relative energies are calculated at the MC-QCISD//MP2/6-311+G(d,p) + ZPE level (in kcal mol^{-1}). Values in parentheses are calculated at the MP2/6-311+G(d,p) + ZPE level

curvature tunneling (SCT) contributions in a wide temperature range of 200–1,500 K. The CVT/SCT rate constants of $k_{1a\text{-}4a}$ are given in Tables 4 and 5 along with the available experimental results [14–16]. The calculated rate constant values of k_{2a}, k_{3a}, and k_{4a} were in good agreement with the available experimental values [14–16]. For example, the ratios of $k_{CVT/SCT}/k_{expt.}$ were 0.99 at 470 K, 1.05 at 500 K, and 1.42 at 425 K, respectively. The theoretical CVT/SCT rate constant of reaction channel $CF_3 + SiHF_3 \rightarrow SiF_3 + CHF_3$ (R1a) was 3.28×10^{-15} $cm^3molecule^{-1}s^{-1}$, which is smaller than that of reaction channel $CH_3 + SiHF_3 \rightarrow SiF_3 + CH_4$ (R2a) (3.31×10^{-16} $cm^3molecule^{-1}s^{-1}$) at 470 K. Theoretical activation energy (E_a) is estimated based on the calculated CVT/SCT rate constants, and the corresponding E_a value for reaction channel R1a, 3.86 kcal mol^{-1}, was found to be lower than that for reaction channel R2a (5.00 kcal mol^{-1}) in 350–500 K, which is in accordance with its kinetic superiority. These results are consistent with a qualitative assessment based on the potential energy barrier heights of

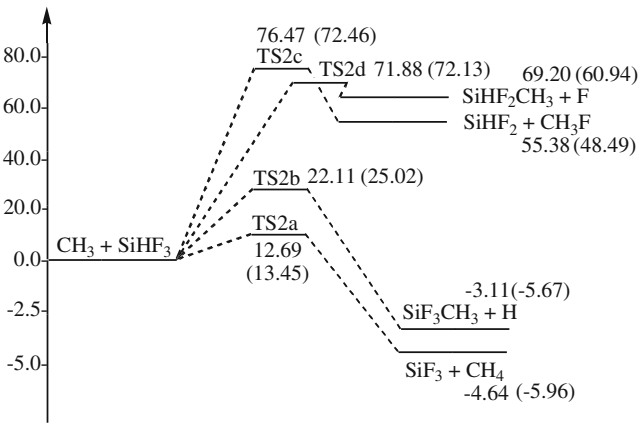

Fig. 3 Schematic potential energy surface for the reaction CH_3 + $SiHF_3$. Relative energies are calculated at the MC-QCISD//MP2/6-311+G(d,p) + ZPE level (in kcal mol^{-1}). Values in parentheses are calculated at the MP2/6-311+G(d,p) + ZPE level

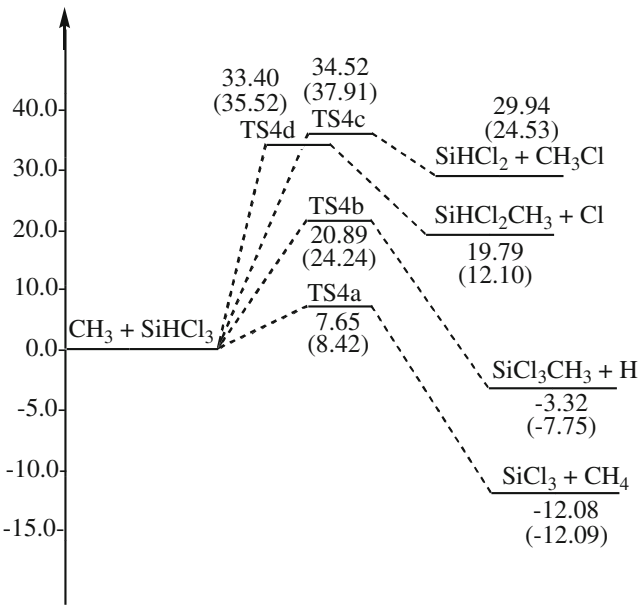

Fig. 5 Schematic potential energy surface for the reaction CH_3 + $SiHCl_3$. Relative energies are calculated at the MC-QCISD//MP2/6-311+G(d,p) + ZPE level (in kcal mol^{-1}). Values in parentheses are calculated at the MP2/6-311+G(d,p) + ZPE level

Table 4 Calculated transition state theory (TST), canonical variational transition state theory (CVT), CVT/small-curvature tunneling (SCT) rate constants ($cm^3molecule^{-1}s^{-1}$) of the reaction channel R1a, k_{1a}, and R2a, k_{2a}, in the temperature range 200—1,500 K at the MC-QCISD//MP2/6-311+G(d,p) level together with the corresponding experimental value

T(K)	k_{1a}(TST)	k_{1a}(CVT)	k_{1a}(CVT/SCT)	k_{2a}(TST)	k_{2a}(CVT)	k_{2a}(CVT/SCT)	k [14]
200	2.56×10^{-14}	2.25×10^{-14}	3.49×10^{-17}	5.63×10^{-17}	5.50×10^{-17}	5.43×10^{-19}	
225	2.91×10^{-14}	2.62×10^{-14}	6.92×10^{-17}	1.15×10^{-16}	1.13×10^{-16}	1.68×10^{-18}	
250	3.36×10^{-14}	3.07×10^{-14}	1.28×10^{-16}	2.05×10^{-16}	2.02×10^{-16}	4.25×10^{-18}	
295	4.39×10^{-14}	4.10×10^{-14}	3.29×10^{-16}	4.67×10^{-16}	4.62×10^{-16}	1.60×10^{-17}	
343	5.85×10^{-14}	5.54×10^{-14}	7.60×10^{-16}	9.14×10^{-16}	9.06×10^{-16}	4.71×10^{-17}	1.06×10^{-17}
350	6.09×10^{-14}	5.78×10^{-14}	8.49×10^{-16}	9.95×10^{-16}	9.87×10^{-16}	5.40×10^{-17}	1.37×10^{-17}
400	8.11×10^{-14}	7.67×10^{-14}	1.43×10^{-15}	1.71×10^{-15}	1.70×10^{-15}	1.28×10^{-16}	6.53×10^{-17}
450	1.06×10^{-13}	9.92×10^{-14}	2.63×10^{-15}	2.67×10^{-15}	2.65×10^{-15}	2.58×10^{-16}	2.20×10^{-16}
470	1.18×10^{-13}	1.10×10^{-13}	3.28×10^{-15}	3.13×10^{-15}	3.11×10^{-15}	3.31×10^{-16}	3.34×10^{-16}
500	1.37×10^{-13}	1.37×10^{-13}	4.48×10^{-15}	3.90×10^{-15}	3.89×10^{-15}	4.67×10^{-16}	
525	1.55×10^{-13}	1.42×10^{-13}	5.72×10^{-15}	4.64×10^{-15}	4.62×10^{-15}	6.07×10^{-16}	
600	2.19×10^{-13}	1.99×10^{-13}	1.10×10^{-14}	7.33×10^{-15}	7.31×10^{-15}	1.21×10^{-15}	
700	3.32×10^{-13}	2.98×10^{-13}	2.32×10^{-14}	1.22×10^{-14}	1.22×10^{-14}	2.57×10^{-15}	
800	4.84×10^{-13}	4.31×10^{-13}	4.37×10^{-14}	1.89×10^{-14}	1.88×10^{-14}	4.75×10^{-15}	
900	6.81×10^{-13}	6.03×10^{-13}	7.56×10^{-14}	2.75×10^{-14}	2.75×10^{-14}	8.00×10^{-15}	
1,000	9.29×10^{-13}	8.19×10^{-13}	1.22×10^{-13}	3.84×10^{-14}	3.83×10^{-14}	1.26×10^{-14}	
1,200	1.61×10^{-12}	1.41×10^{-12}	2.77×10^{-13}	6.80×10^{-14}	6.80×10^{-14}	2.66×10^{-14}	
1,500	3.20×10^{-12}	2.79×10^{-12}	7.31×10^{-13}	1.36×10^{-13}	1.36×10^{-13}	6.37×10^{-14}	

the two reaction channels. A similar sequence was found for the other two reaction channels R3a and R4a.

We hope that our present study will extend experimental knowledge on the kinetics of the title reaction and provide

Table 5 Calculated TST, CVT, CVT/SCT rate constants ($cm^3molecule^{-1}s^{-1}$) of the reaction channel R3a, k_{3a}, and R4a, k_{4a}, in the temperature range 200—1,500 K at the MC-QCISD//MP2/6-311+G(d,p) level together with the corresponding experimental values

T(K)	k_{3a}(TST)	k_{3a}(CVT)	k_{3a}(CVT/SCT)	k [15]	k_{4a}(TST)	k_{4a}(CVT)	k_{4a}(CVT/SCT)	k [16]
200	4.27×10^{-14}	1.75×10^{-14}	3.55×10^{-17}		2.73×10^{-15}	1.24×10^{-15}	2.92×10^{-17}	
225	3.91×10^{-14}	1.69×10^{-14}	6.24×10^{-17}		3.67×10^{-15}	1.69×10^{-15}	5.14×10^{-17}	
250	3.77×10^{-14}	1.69×10^{-14}	1.03×10^{-16}		4.74×10^{-15}	2.20×10^{-15}	9.00×10^{-17}	
295	3.82×10^{-14}	1.81×10^{-14}	2.22×10^{-16}		6.93×10^{-15}	3.24×10^{-15}	2.04×10^{-16}	
343	4.13×10^{-14}	2.03×10^{-14}	4.38×10^{-16}		9.66×10^{-15}	4.55×10^{-15}	4.04×10^{-16}	
350	4.19×10^{-14}	2.07×10^{-14}	4.79×10^{-16}	1.44×10^{-16}	1.01×10^{-14}	4.76×10^{-15}	4.42×10^{-16}	2.34×10^{-16}
400	4.71×10^{-14}	2.39×10^{-14}	8.57×10^{-16}	4.40×10^{-16}	1.34×10^{-14}	6.36×10^{-15}	7.75×10^{-16}	5.07×10^{-16}
425	5.03×10^{-14}	2.58×10^{-14}	1.11×10^{-15}	6.95×10^{-16}	1.53×10^{-14}	7.26×10^{-15}	9.89×10^{-16}	6.97×10^{-16}
450	5.38×10^{-14}	2.79×10^{-14}	1.41×10^{-15}	1.05×10^{-15}	1.73×10^{-14}	8.21×10^{-15}	1.24×10^{-15}	
470	5.69×10^{-14}	2.97×10^{-14}	1.69×10^{-15}	1.50×10^{-15}	1.89×10^{-14}	9.01×10^{-15}	1.47×10^{-15}	
500	6.19×10^{-14}	3.27×10^{-14}	2.19×10^{-15}	2.09×10^{-15}	2.16×10^{-14}	1.03×10^{-14}	1.85×10^{-15}	
525	6.64×10^{-14}	3.53×10^{-14}	2.67×10^{-15}	2.82×10^{-15}	2.40×10^{-14}	1.14×10^{-14}	2.22×10^{-15}	
600	8.22×10^{-14}	4.43×10^{-14}	4.55×10^{-15}		3.20×10^{-14}	1.53×10^{-14}	3.61×10^{-15}	
700	1.08×10^{-13}	5.92×10^{-14}	8.29×10^{-15}		4.50×10^{-14}	2.15×10^{-14}	6.18×10^{-15}	
800	1.41×10^{-13}	7.74×10^{-14}	1.37×10^{-14}		6.09×10^{-14}	2.92×10^{-14}	9.70×10^{-15}	
900	1.80×10^{-13}	9.94×10^{-14}	2.12×10^{-14}		7.99×10^{-14}	3.83×10^{-14}	1.43×10^{-14}	
1,000	2.26×10^{-13}	1.25×10^{-13}	3.11×10^{-14}		1.02×10^{-13}	4.90×10^{-14}	2.02×10^{-14}	
1,200	3.42×10^{-13}	1.91×10^{-13}	5.93×10^{-14}		1.58×10^{-13}	7.59×10^{-14}	3.61×10^{-14}	
1,500	5.82×10^{-13}	3.24×10^{-13}	1.27×10^{-13}		2.74×10^{-13}	1.31×10^{-13}	7.22×10^{-14}	

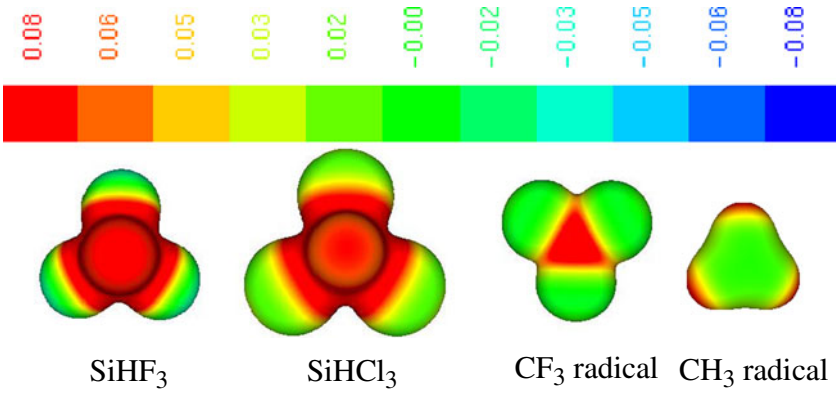

Fig. 6 Calculated electrostatic potential textured van der Waals surfaces for the reactants. The most negative and positive potentials are indicated in *blue* and *red*, respectively, and the color spectrum is mapped to all other values by linear interpolation

useful information for future experimental measurements. The three-parameter fits of the CVT/SCT rate constants of the four reaction channels in the temperature range from 200 to 1,500 K were performed and the expressions are given as follows (in units of $cm^3 molecule^{-1} s^{-1}$):

$$k_{1a}(T) = 2.93 \times 10^{-26} T^{4.25} \exp(-318.68/T)$$

$$k_{2a}(T) = 3.67 \times 10^{-22} T^{2.72} \exp(-1414.22/T)$$

$$k_{3a}(T) = 7.00 \times 10^{-24} T^{3.27} \exp(-384.04/T)$$

$$k_{4a}(T) = 6.35 \times 10^{-22} T^{2.59} \exp(-603.18/T)$$

Reactivity trends

The molecular electrostatic potential is an important tool used to analyze molecular reactivity because it can provide information about local polarity. Figure 6 presents the distribution of the molecular electrostatic potential. There, the most negative and positive potentials are indicated in blue and red, respectively, and the color spectrum is mapped to all other values by linear interpolation. The more negative potential region (more blue) will be more favored for electrophilic attack. In the molecules trifluoro- and trichloro-silane, the H atoms bear stronger positive potential (red) than the halogen atoms (green), indicating that the H atoms can be attacked more easily by the nucleophile. Note that the C atom of CF_3 radical is encircled by marked negative potential; therefore, the CF_3 radical preferentially attacks the H atom in $SiHF_3$ and $SiHCl_3$ compared to the CH_3 group. From these results, we can infer that the H-abstraction reaction channel and halogen-abstraction reaction channel in $SiHF_3$ and $SiHCl_3$ with the CF_3 radical could occur more easily than with the CH_3 radical. As a result, the reaction rate constants increase in the order of $CH_3 + SiHX_3 < CF_3 + SiHX_3$ (X = F, Cl). This is in line with the potential energy barrier heights, bond dissociation energies, and the rate constant results calculated above.

Conclusions

In this paper, the multi-channel reactions $SiHX_3$ (F, Cl) with CF_3 and CH_3 radicals were investigated theoretically using direct dynamics methods. Four type reaction pathways were identified; H-abstraction, F-abstraction, H-displacement and F-displacement from $SiHF_3$ for the four reactions. The calculated potential barriers show that major reaction channel is H-abstraction. The results of theoretical investigation mean that for the four reactions, the H-abstraction reaction rate constants decrease in the order of $CF_3 + SiHX_3 > CH_3 + SiHX_3$ (X = F, Cl). The calculated results are in good agreement with the corresponding available experimental values. We expect that the theoretical results may be useful for estimating the kinetics of the reactions over a wide temperature range where no experimental data is available

Acknowledgments The authors thank Professor Donald G. Truhlar for providing the POLYRATE 9.7 program. This work was supported by the National Natural Science Foundation of China (20973077 and 20973049), the Program for New Century Excellent Talents in University (NCET), the Doctoral Fund of Ministry of Education of China (20112303110005), the Foundation for the Department of Education of Heilongjiang Province (1152G010, 11551077), the Key Subject of Science and Technology by the Ministry of Education of China, the SF for leading experts in academe of Harbin of China (2011RFJGS026), the Science Foundation for Distinguished Young Scholar of Heilongjiang Province (JC201206).

References

1. Fester GW, Eckstein J, Gerlach D, Wagler J, Brendler E, Kroke E (2010) Inorg Chem 49:2667–2673
2. Giraldo OH, Willis WS, Márquez M, Suib SL, Hayashi Y, Matsumoto H (1998) Chem Mater 10:366–371
3. Valente G, Cavallotti C, Masi M, Carrà S (2001) J Cryst Growth 230:247–257
4. Reznik B, Gerthsen D, Zhang WG, Hüttinger KJ (2003) J Eur Ceram Soc 23:1499–1508

5. Yang Y, Zhang WG (2009) Chin J Chem Eng 17:419–426
6. Zhang P, Wang WW, Cheng GH, Li JL (2011) Chin J Chem Eng 19:1–9
7. Schlegel HB (1984) J Phys Chem 88:6254–6258
8. Zhang WG, Hüttinger KJ (2001) Chem Vap Depos 7:173–181
9. Lee JY, Lee WH, Park YK, Kim HY, Kang NY, Yoon KB, Choi WC, Yang OB (2012) Sol Energy Mater Sol Cells 105:142–147
10. Koinuma H, Manako T, Natsuaki H, Fujioka H, Fueki K (1985) J Non-Cryst Solids 77:801–804
11. Matsuda A, Yagii K, Kaga T, Tanaka K (1984) Jpn J Appl Phys 23: L576–L578
12. Robertson R, Hils D, Gallagher A (1984) Chem Phys Lett 103:397–404
13. Longeway PA, Estes RD, Weakliem HA (1984) J Phys Chem 88:73–77
14. Kerr JA, Slater DH, Young JC (1967) J Chem Soc A 134–137
15. Arthur NL, Bell TN (1978) Rev Chem Intermed 2:37–74
16. Kerr JA, Stephens A, Young JC (1969) Int J Chem Kinet 1:371–380
17. Arthur NL, Christie JR, Mitchell GD (1979) Aust J Chem 32:1017–1023
18. Bell TN, Johnson BB (1967) Aust J Chem 20:1545–1551
19. Kerr JA, Slater DH, Young JC (1966) J Chem Soc A 104–108
20. Bell RL, Truong TN (1994) J Chem Phys 101:10442–10451
21. Truong TN, Duncan WT, Bell RL (1996) Chemical applications of density functional theory. American Chemical Society, Washington, DC, p 85
22. Truhlar DG (1995) In: Heidrich D (ed) The reaction path in chemistry:current approaches and perspectives. Kluwer, Dordrecht
23. Corchado JC, Espinosa-Garcia J, Hu W-P, Rossi I, Truhlar DG (1995) J Phys Chem 99:687–694
24. Hu W-P, Truhlar DG (1996) J Am Chem Soc 118:860–869
25. Fast PL, Truhlar DG (2000) J Phys Chem A 104:6111–6116
26. Corchado JC, Chuang Y-Y, Fast PL, Hu W-P, Liu Y-P, Lynch GC, Nguyen KA, Jackels CF, Fernandez-Ramos A, Ellingson BA, Lynch BJ, Zheng JJ, Melissasa VS, Villa J, Rossi I, Coitino EL, Pu JZ, Albu TV, Steckler R, Garrett BC, Isaacson AD, Truhlar DG (2007) POLYRATE version 9.7. Department of Chemistry and Supercomputer Institute, University of Minnesota, Minneapolis
27. Truhlar DG, Garrett BC (1980) Acc Chem Res 13:440–448
28. Truhlar DG, Isaacson AD, Garrett BC (1985) Generalized transtion state theory. In: Baer M (ed) The theory of chemical reaction dynamics, 4th edn. CRC, Boca Raton, p 65
29. Duncan WT, Truong TN (1995) J Chem Phys 103:9642–9652
30. Frisch MJ, Head-Gordon M, Pople JA (1990) Chem Phys Lett 166:275–280
31. Head-Gordon M, Pople JA, Frisch MJ (1988) Chem Phys Lett 153:503–506
32. Boris B, Petia B (1999) J Phys Chem A 103:6793–6799
33. Bergman DL, Laaksonen L, Laaksonen A (1997) J Mol Graph Model 15:301–306
34. Frisch MJ, Trucks GW, Schlegel HB, Scuseria GE, Robb MA, Cheeseman JR, Scalmani G, Barone V, Mennucci B, Petersson GA, Nakatsuji H, Caricato M, Li X, Hratchian HP, Izmaylov AF, Bloino J, Zheng G, Sonnenberg JL, Hada M, Ehara M, Toyota K, Fukuda R, Hasegawa J, Ishida M, Nakajima T, Honda Y, Kitao O, Nakai H, Vreven T, Montgomery JA, Jr, Peralta JE, Ogliaro F, Bearpark M, Heyd JJ, Brothers E, Kudin KN, Staroverov VN, Kobayashi R, Normand J, Raghavachari K, Rendell A, Burant JC, Iyengar SS, Tomasi J, Cossi M, Rega N, Millam JM, Klene M, Knox JE, Cross JB, Bakken V, Adamo C, Jaramillo J, Gomperts R, Stratmann RE, Yazyev O, Austin AJ, Cammi R, Pomelli C, Ochterski JW, Martin RL, Morokuma K, Zakrzewski VG, Voth GA, Salvador P, Dannenberg JJ, Dapprich S, Daniels AD, Farkas O, Foresman JB, Ortiz JV, Cioslowski J, Fox DJ (2009) Gaussian, Inc., Revision A.02, Wallingford CT
35. Garrett BC, Truhlar DG (1979) J Chem Phys 70:1593–1598
36. Garrett BC, Truhlar DG (1979) J Am Chem Soc 101:4534–4548
37. Garrett BC, Truhlar DG, Grev RS, Magnuson AW (1980) J Phys Chem 84:1730–1748
38. Lu DH, Truong TN, Melissas VS, Lynch GC, Liu Y-P, Grarrett BC, Steckler R, Issacson AD, Rai SN, Hancock GC, Lauderdale JG, Joseph T, Truhlar DG (1992) Comput Phys Commun 71:235–262
39. Liu Y-P, Lynch GC, Truong TN, Lu D-H, Truhlar DG, Garrett BC (1993) J Am Chem Soc 115:2408–2415
40. Truhlar DG (1991) J Comput Chem 12:266–270
41. Chuang YY, Truhlar DG (2000) J Chem Phys 112:1221–1228
42. Kuchitsu K (1998) Structure of free polyatomic molecules basic data. Springer, Berlin, pp 84, 87, 102, 104, 105, 111
43. Hammond GS (1955) J Am Chem Soc 77:334–338
44. Jacox ME (2005) In: NIST Chemistry WebBook, NIST Standard Reference Database Number 69, June, Release
45. Shimanouchi T (2005) In: NIST Chemistry WebBook, NIST Standard Reference Database Number 69, June, Release
46. Chase MW (1998) NIST-JANAF Themochemical Tables, 4th ed., J Phys Chem Ref Data, Monograph 9, ACS: Washington, DC 1–1951
47. Afeefy HY, Liebman JF, Stein SE (2005) In: NIST ChemistryWebBook, NIST Standard Reference Database Number 69, June, R
48. Ho P, Melius CF (1990) J Phys Chem 94:5120–5127
49. Manion JA (2002) J Phys Chem Ref Data 123–172
50. Doncaster AM, Walsh R (1978) Int J Chem Kinet 10:101–110
51. Wu YD, Wong CL (1995) J Org Chem 60:821–828
52. Walsh R (1989) In: Patai S, Rapport Z (eds) Thermochemistry. In: The chemistry of organo silicon compounds, Part 1, vol Chapter 5. Wiley, New York, pp 371–391
53. Hildenbrand DL, Lau KH, Sanjurjo A (2003) J Phys Chem A 107:5448–5451
54. Becerra R, Walsh R (1998) Thermochemistry. In: Rapport Z, Apeloig Y (eds) The chemistry of organic silicon compounds Vol 2, vol Chapter 4. Wiley, New York, pp 153–180